Journal Pre-proofs

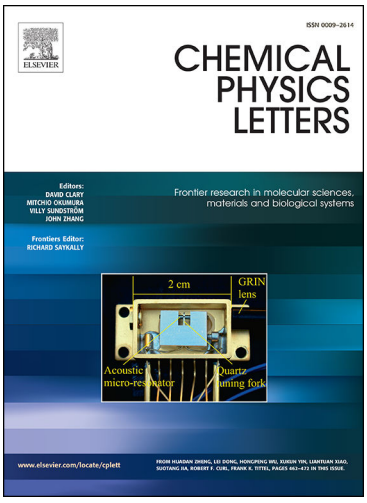

Research paper

Near-Infrared Reversible Photoswitching of an Isolated Azobenzene-Stilbene Dye

Eduardo Carrascosa, James N. Bull, Jack T. Buntine, Gabriel da Silva, Paulo F. Santos, Evan J. Bieske

PII: S0009-2614(19)31046-2
DOI: https://doi.org/10.1016/j.cplett.2019.137065
Reference: CPLETT 137065

To appear in: *Chemical Physics Letters*

Received Date: 16 November 2019
Revised Date: 21 December 2019
Accepted Date: 28 December 2019

Please cite this article as: E. Carrascosa, J.N. Bull, J.T. Buntine, G. da Silva, P.F. Santos, E.J. Bieske, Near-Infrared Reversible Photoswitching of an Isolated Azobenzene-Stilbene Dye, *Chemical Physics Letters* (2019), doi: https://doi.org/10.1016/j.cplett.2019.137065

This is a PDF file of an article that has undergone enhancements after acceptance, such as the addition of a cover page and metadata, and formatting for readability, but it is not yet the definitive version of record. This version will undergo additional copyediting, typesetting and review before it is published in its final form, but we are providing this version to give early visibility of the article. Please note that, during the production process, errors may be discovered which could affect the content, and all legal disclaimers that apply to the journal pertain.

© 2019 Published by Elsevier B.V.

evanjb@unimelb.edu.au
[1]School of Chemistry, The University of Melbourne, Parkville, Victoria 3010, Australia [2]Laboratoire de Chimie Physique Moléculaire, École Polytechnique Fédérale de Lausanne, EPFL SB ISIC LCPM, Station 6, CH-1015 Lausanne, Switzerland [3]School of Chemistry, Norwich Research Park, University of East Anglia, Norwich NR4 7TJ, United Kingdom [4]Department of Chemical Engineering, University of Melbourne, Parkville, VIC 3010, Australia [5]Centro de Química - Vila Real, Universidade de Trás-os-Montes e Alto Douro, 5001-801 Vila Real, Portugal

Photoswitching of a charged azobenzene-stilbene dye is investigated through laser excitation in a tandem ion mobility mass spectrometer. Action spectra associated with $E \rightarrow Z$ and $Z \rightarrow E$ photoisomerisation of the stilbene group exhibit bands at 685 and 440 nm, corresponding to $S_1 \leftarrow S_0$ and $S_3 \leftarrow S_0$ transitions, respectively. The data suggest that isomers possessing a *Z* configuration of the azobenzene unit rapidly convert to *E* isomers and are not discernible using ion mobility spectrometry, and that photoisomerisation occurs through excited state dynamics rather than statistical isomerisation on the ground state potential energy surface.

photoswitch photoisomerisation stilbene ion mobility action spectroscopy

1 Introduction

Near-infrared (NIR) photoswitches are appealing for medical and pharmacological applications because biological tissue is relatively transparent to NIR light [1]. One interesting class of `hybrid' NIR photoswitches combines cationic azo-dye and stilbene units [2], both of which are common constituents of molecular photoswitches and light-driven molecular machines [3, 4, 5]. Such hybrid photoswitches operate in polar solvents and potentially possess four distinct geometric isomers, allowing for large changes in the structures of grafted molecules. The inherent photoswitching characteristics of hybrid photoswitches can be investigated by first isolating a target isomer using HPLC, irradiating the sample, and then characterising the photoproduct using HPLC or NMR. However, sub-second thermal reversion of the less stable isomers at room temperature, a desirable characteristic for pharmacological applications, restricts the suitability of such conventional approaches.

Here, we investigate a hybrid NIR photoswitch denoted DTVE (2-2-[4-chloro-2-(4-diethylaminophenylazo)thiazol-5-yl]-vinyl-1-ethylquinolinium], Figure 1(a)) using photoisomerisation action spectroscopy (PISA spectroscopy), a technique that allows the selection and characterisation of a target isomer ion in the gas phase [6, 7]. The approach, which is applicable for charged molecular photoswitches, combines a first ion mobility stage - a zone in which the drifting ions are exposed to tunable radiation - and a second ion mobility stage in which the resulting photoisomers are separated [6, 7]. In ion mobility spectrometry (IMS), charged molecules propelled by an electric field through a buffer gas are separated according to their drift speeds, which depend on their collision cross-sections [8]. Folded,

compact ions traverse the drift region more rapidly than unfolded, extended ions. In PISA spectroscopy, the target isomer is selected in a primary IMS stage and then exposed to light of tunable wavelength, with separation of photoisomers or photofragments in a second IMS stage. The inherent isomer selectivity avoids complications associated with overlapping spectra of coexisting isomers that potentially bedevil other gas-phase spectroscopic techniques.

Figure 1: (a) Structure of DTVE. (b) Ground electronic state potential energy surface of DTVE with calculated isomerisation barriers (transition states) connecting the four isomers and calculated collision cross sections (Ω_c) for each isomer given in units of $Å^2$. The isomer labelling (*EE*, *EZ*, *ZE* or *ZZ*) refers first to the azo group and second to the stilbene group.

2 Methods

2.1 Experimental approach

Figure 2: Tandem ion mobility spectrometer used to study photoisomerisation of DTVE. Electrosprayed ions are gathered by an ion funnel (IF1), and are injected into the first ion mobility stage (IMS1) through the first ion gate (IG1). After passing through IMS1 a particular isomer can be gated by a second ion gate (IG2) before passing through the second ion mobility stage (IMS2) and being gathered by a second ion funnel (IF2). The ions then pass through an octupole ion guide (oct) and quadrupole mass filter (QMF) before encountering a channeltron ion detector.

Photoisomerisation of the DTVE isomer ions was investigated using a tandem ion mobility spectrometer shown in Figure 2 that has been described elsewhere [6, 7]. The instrument consists of two ion mobility drift regions (IMS1 and IMS2) and a quadrupole mass filter (QMF). A sample of DTVE dissolved in methanol (≈ 10 μM) was electrosprayed into an RF ion funnel (IF1), which radially gathered and confined the ions. An ion gate (IG1) at the end of IF1 injected 100 μs packets of ions into IMS1. In the drift region, the ions were propelled by an electric field (≈ 44 V cm^{-1}) through N_2 buffer gas (≈ 6 Torr), such that isomers were separated in time and space according to their collision cross-sections with N_2. At the end of IMS2, the ions were radially confined using another ion funnel (IF2), passed through a octupole ion guide, were mass selected by the QMF and then detected with a Channeltron. The detector was connected to a multichannel scaler to generate an arrival time distribution (ATD) as a histogram of ion count against arrival time. Peaks in the ATD correspond to particular isomers. The mobility resolution of the combined IMS stages (IMS1+IMS2) is ≈ 80.

For the photoisomerisation experiments, the target isomer packet was selected using a Bradbury-Nielsen ion gate (IG2) situated between IMS1 and IMS2. Immediately after gating, the target isomer population was irradiated with tunable light from an optical parametric oscillator

(OPO, EKSPLA NT342B). Resulting photoisomers were separated from the parent isomer during their passage through IMS2. The OPO was operated at 20 Hz, half the ion injection frequency, allowing accumulation of light-on and light-off ATDs. The difference between these ATDs (i.e. light-on -- light-off) yielded a photoaction ATD, that reflects the influence of light on the ions' structures -- see examples in Ref. [6]. A PISA spectrum was derived by plotting the photoisomer yield as a function of wavelength and normalising with respect to light fluence and light-off signal. The light intensity was kept at low levels ($\approx$0.2 mJ cm^{-2} pulse^{-1}) to avoid multiphoton absorption and sequential isomerisations. The photoisomer yield was less than 5% across the studied wavelength range and there was no evidence for photodissociation.

2.2 Theoretical approach

Electronic structure calculations were performed at the ωB97X-D/cc-pVDZ level of theory[9, 10] using Gaussian 16 [11] to determine the DTVE isomer geometries, relative energies, harmonic vibrational frequencies, and isomerisation transition states. Vertical electronic excitation energies were computed at the df-CC2/cc-pVDZ (cc-pVDZ-RI auxiliary basis set) level of theory using MRCC (May 2018 release) [12]. Natural transition orbitals asociated with the $S_1 \leftarrow S_0$ and $S_3 \leftarrow S_0$ transitions were computed for the *EE* isomer at the (TD-DFT) ωB97X-D/cc-pVDZ level of theory to gauge the charge-transfer character of the transitions [13].

Collision cross-sections for the DTVE isomers were calculated using MOBCAL with the trajectory method parameterized for N_2 buffer gas [14, 15]. Input charge distributions were computed at the ωB97X-D/cc-pVDZ level of theory with the Merz-Singh-Kollman scheme constrained to reproduce the electric dipole moment [16]. Sufficient trajectories were computed such that the calculated values had standard deviations of ± 1 Å^2. Calculated collision cross-sections do not account for rotamers (i.e. rotations about single bonds) or fluxionality of the ions in the drift region.

Statistical isomerisation of the DTVE isomers on the ground state potential energy surface was investigated through master equation simulations using the MultiWell suite of programs [17, 18, 19]. Microscopic rate coefficients were calculated with Rice-Ramsperger-Kassel-Marcus (RRKM) theory using sums and densities of states from the Stein-Rabinovitch-Beyer-Swinehart algorithm. Vibrational and rotational degrees of freedom were treated using the harmonic-oscillator and rigid-rotor symmetric top approximations. Time-dependent master equation simulations used a hybrid energy-grained approach, assuming 4 000 energy grains of 10 cm^{-1} followed by a continuum regime up to 200 000 cm^{-1}. Simulations were performed for $\approx 10^6$ trajectories. The MultiWell code was modified to treat ion-molecule collisions with the Langevin model. Simulations for photoactivated ions used thermal energy distributions at 300 K offset by the energy of the absorbed photon [20]. The Langevin model assumed 100 cm^{-1} of energy is quenched per deactivating collision until thermal equilibrium is reached.

3 Results and Discussion

3.1 ATDs and isomer assignment

DTVE has four geometric isomers (*EE*, *EZ*, *ZE* and *ZZ*) corresponding to the *E/Z* configuration of the respective stilbene and azo bonds (see Figure 1a for the labelling scheme). ATDs for electrosprayed DTVE are shown in Figure 3. Under gentle operating conditions (low RF drive voltage to IF1) only one ATD peak was observed (at 19.6 ms), which likely corresponds to the most stable *EE* isomer (see Figure 1b). Collisional activation of the ions, achieved by applying a high RF drive voltage to the source ion funnel (IF1 high), promoted formation of a more compact isomer arriving at $\approx$19.0 ms, most convincingly assigned to the next most stable isomer, *EZ*. There is no evidence in the ATD for the *ZE* and *ZZ* isomers, which are predicted to lie much higher in energy and are separated from the *EE* and *EZ* isomers by relatively low barriers (Figure 1b), and so are less likely to survive in the drift region (interconversion of these isomers is discussed below in Section 3.3). Even if the *ZE* and *ZZ* isomers did survive passage through the drift region, their calculated collision cross sections are similar to those of the *EE* and *EZ* isomers, respectively, potentially making them difficult to distinguish in the ATD (see Ω_c values in Figure 1a).

Exposure of the DTVE in methanol solution to either red, green, blue or near-UV light from a high-power light emitting diode for several seconds prior to being electrosprayed produced no discernible change to the `IF1 off' ATD, suggesting that any photoisomers formed in solution thermally revert to the *EE* isomer within a few seconds [21]. The same conclusion was reached through UV-Vis spectrophotometry since the absorption spectrum for a solution irradiated with visible or near-UV light for few seconds before the acquisition was identical to the spectrum for a sample shielded from light.

Figure 3: Arrival time distributions (ATDs) for electrosprayed DTVE obtained with low and high RF drive voltage applied to the source ion funnel.

3.2 PISA spectra of EE and EZ isomers

Figure 4: (a) Absorption spectra of DTVE in methanol and water solutions. (b) Gas-phase PISA spectrum for the DTVE *EE* isomer. (c) Gas-phase PISA spectrum for the DTVE *EZ* isomer. The PISA spectra were accumulated at low light fluence ($\approx$0.2 mJ cm^{-2} pulse^{-1}).

The absorption spectra for DTVE in methanol and water are shown in Figure 4a. The band wavelengths and intensities correspond reasonably well with df-CC2/cc-pVDZ calculations, which predict that for the *EE* isomer the $S_1 \leftarrow S_0$ transition occurs at 666 nm (oscillator strength, $f = 2.7$) and the $S_3 \leftarrow S_0$ transition at 411 nm ($f = 0.3$), respectively. Both transitions have $\pi\pi^*$ character and involve some degree of charge transfer from the dialkylamino-azoarene group to the stilbene group (which carries a net positive charge for the cation in the ground electronic state). Natural transition orbitals for the two transitions are

shown in Figure 5. The $S_2 \leftarrow S_0$ transition, calculated to lie at 512 nm, is optically forbidden. As for the solution spectra, the *EE*$\rightarrow$*EZ* PISA spectrum, shown in Figure 4b, exhibits two bands centered at 680 nm and 440 nm, shifted to longer wavelength by $\approx$40 nm relative to the methanol solution spectrum bands. The blue shift of the solution absorption spectrum compared with the gas-phase action spectrum is consistent with charge-transfer character of the transitions and solvent-induced stabilisation of the occupied π orbitals. Interestingly, the $S_3 \leftarrow S_0$ band in the PISA spectrum is relatively more intense than in the solution absorption spectrum and predicted by the calculations, indicating that in the gas phase the photoisomerisation quantum yield may be roughly an order of magnitude larger for the S_3 state than for the S_1 state. The *EZ*$\rightarrow$*EE* PISA spectrum shown in Figure 3c exhibits bands at 640 and 470 nm, consistent with df-CC2/cc-pVDZ predictions for the $S_1 \leftarrow S_0$ transition at 666 nm ($f = 1.7$) and $S_3 \leftarrow S_0$ transition at 441 nm ($f = 0.8$). Again, the $S_2 \leftarrow S_0$ transition, calculated to lie at 495 nm, is optically forbidden. The shorter wavelength PISA band is more intense than the longer wavelength band, also suggesting that the S_3 state has a higher isomerisation yield than the S_1 state.

Figure 5: Natural transition orbitals for the *EE* isomer of DTVE. The $S_1 \leftarrow S_0$ and $S_3 \leftarrow S_0$ transitions both involve some degree of charge transfer.

3.3 Role of ground state statistical isomerisation

Figure 6: Master equation simulations of the abundances of (a) *ZE* and (b) *ZZ* isomers of DTVE with time at 300 K. In both cases, there is rapid thermal interconversion to give predominately *EE* ions.

	product isomer %			
	EE	*ZE*	*EZ*	*ZZ*
↓ initial isomer	300 K			
EE	100	0	0	0
ZE	86	14	0	0
EZ	0	0	100	0
ZZ	90	10	0	0
	300 K + 680 nm photon			
EE	100	0	0	0

Journal Pre-proofs

ZE	99	0	1	0
EZ	0	0	100	0
ZZ	92	0	8	0
	300 K + 440 nm photon			
EE	100	0	0	0
ZE	96	0	4	0
EZ	9	0	91	0
ZZ	82	0	18	0

Table 1: Predicted abundance of DTVE product isomers in the ion mobility drift region folllowing generation of a statistical ensemble of *EE*, *ZE*, *EZ* or *ZZ* ions (each row) at 300 K, 300 K plus 680 nm photon energy, and 300 K plus 440 nm photon energy. Master equation simulations were run for ≈ 10 μs, sufficiently long to approach thermalisation in all cases. The drift time of the ions in the experiment (≈ 20 ms) is around 3 orders of magnitude longer than the duration of the simulation.

It is clear that the *EE* and *EZ* isomers undergo reversible photoisomerisation in the gas phase. Photoisomerisation of DTVE is likely to occur *via* two mechanisms: (i) rapid isomerisation by passage of the excited state molecule through a conical intersection at a geometry intermediate between those for the *E* and *Z* isomers, and (ii) statistical rearrangement of energised molecules on the ground electronic state potential energy surface by traversing the isomerisation barrier. To help understand the importance of the latter processes - statistical isomerisation on the ground state potential energy surface - we performed master equation simulations using RRKM rates for statistical isomerisations (see transition state barriers in Figure 1b) and a Langevin ion-molecule collision model describing collisional energy transfer with the buffer gas [20].

We first investigated isomerisation of the *ZE* and *ZZ* isomers, assuming a temperature of 300 K, to decide whether these isomers survive the passage through the ion mobility drift region or whether they convert to the more stable *EE* and *EZ* forms. Relative abundances of each isomer plotted against time are shown in Figure 4. The *ZE* and *ZZ* isomers almost completely convert to the *EE* isomer and to a lesser extent the *EZ* isomer within ≈ 20 μs. Because the total drift time in the ion mobility experiment is ≈ 20 ms (see Figure 2a), we conclude that the *ZE* and *ZZ* isomers are unlikely to be observed in our experiments. The *EE* and *EZ* isomers are predicted to be thermally stable at 300 K (Table 1), and, because their calculated collision cross-sections differ by ≈ 6 Å^2, they should be separable in the IMS, in line with the ATDs shown in Figure 3.

To ascertain the relative importance of statistical isomerisation on the ground state potential energy surface following absorption of a photon and internal conversion, we modelled the abundance of each isomer starting from a 300 K ensemble with additional energy provided by a 680 nm or 440 nm photon (these wavelengths correspond to maxima of the first and second PISA bands for the *EE* isomer; see Figure 4b). Results of these simulations are

summarised in Table 1. The modelling predicts that *EE* ions with the additional energy provided by a 680 nm or 440 nm photon undergo collisional cooling before they can statistically isomerise (Table 1). Rapid collisional quenching and negligible isomerisation is also predicted for *EZ* ions possessing additional energy from a 680 nm photon. In contrast, *EZ* ions activated by a 440 nm photon are predicted to statistically convert to the *EE* isomer with a 9% yield. The inefficiency of statistical isomerisation on the ground state potential energy surface predicted for both the *EE* and *EZ* isomers following photon absorption, particularly at longer wavelengths, runs counter to the experimental observation of $EE \rightarrow EZ$ and $EZ \rightarrow EE$ photoisomerisation at 680 nm and 440 nm. This suggests that photoisomerisation does not involve internal conversion followed by rearrangement on the ground state potential energy surface. Rather, photoisomerisation more likely occurs as a non-adiabatic process involving passage through a conical intersection linking the excited and ground state potential energy surfaces. The nascent isomers will then tend to be stabilised and quenched as *EE* and *EZ* isomers through subsequent collisions. Similar conclusions regarding the nature of the photoisomerisation mechanism have been reached for a related azobenzene system in the gas phase [20].

4 Conclusions

Reversible *E-Z* photoisomerisation of a hybrid azobenzene-stilbene photoswitch molecule has been demonstrated in the gas phase using near-infrared and blue-green light. Supporting electronic structure calculations and master equation simulations suggest two (*EE* and *EZ*) of the four possible isomers are thermally stable in the gas phase for at least 20 ms at 300 K. Photoisomerisation of the *EE* and *EZ* isomers appears to involve excited state dynamics of the system, with passage through a conical intersection connecting the excited and ground state, leading to a change in the molecular structure. The present strategy of combining ion mobility mass spectrometry with laser spectroscopy should be suitable to characterise other molecular photoswitches with photopharmacological applications.

Acknowledgments

This research was funded through the Australian Research Council (ARC) Discovery Project scheme (DP150101427 and DP160100474), and Future Fellowship scheme (FT130101304). E.C. acknowledges support by the Austrian Science Fund (FWF) through a Schrödinger Fellowship (Nr. J4013-N36), and J.T.B. acknowledges The University of Melbourne for a Melbourne Research Scholarship (MRS) and the Australian Government for an Australian Research Training Program Scholarship (RTP).

References url urlprefix href

[1] M. Dong, A. Babalhavaeji, S. Samanta, A. A. Beharry, G. A. Woolley, Red-shifting azobenzene photoswitches for *in vivo* use, Acc. Chem. Res. 48 (2015) 2662--2670.

Journal Pre-proofs

[2] M. A. Salvador, P. Almeida, L. Reis, P. Santos, Near-infrared absorbing delocalized cationic azo dyes, Dyes Pig. 82 (2009) 118--123.

[3] B. L. Feringa, The art of building small: From molecular switches to motors (Nobel lecture), Angew. Chem. Int. Ed. 56 (2017) 11060--11078.

[4] W. R. Browne, B. L. Feringa, Light switching of molecules on surfaces, Annu. Rev. Phys. Chem. 60 (2009) 407--428.

[5] D. Bléger, S. Hecht, Visible-light-activated molecular switches, Angew. Chem. Int. Ed. 54 (2015) 11338--11349.

[6] B. D. Adamson, N. J. A. Coughlan, P. B. Markworth, R. E. Continetti, E. J. Bieske, An ion mobility mass spectrometer for investigating photoisomerization and photodissociation of molecular ions, Rev. Sci. Instr. 85 (2014) 123109.

[7] P. B. Markworth, B. D. Adamson, N. J. A. Coughlan, L. Goerigk, E. J. Bieske, Photoisomerization action spectroscopy: flicking the protonated merocyanine--spiropyran switch in the gas phase, Phys. Chem. Chem. Phys. 17 (2015) 25676--25688.

[8] G. A. Eiceman, Z. Karpas, H. H. Hill, Ion Mobility Spectrometry, 3rd Edition, CRC Press, 2013.

[9] J.-D. Chai, M. Head-Gordon, Long-range corrected hybrid density functionals with damped atom-atom dispersion corrections, Phys. Chem. Chem. Phys. 10 (2008) 6615--6620.

[10] T. H. Dunning, Jr., Gaussian basis sets for use in correlated molecular calculations. I. The atoms boron through neon and hydrogen, J. Chem. Phys. 90 (1989) 1007.

[11] M. J. Frisch, G. W. Trucks, H. B. Schlegel, G. E. Scuseria, M. A. Robb, J. R. Cheeseman, G. Scalmani, V. Barone, B. Mennucci, G. A. Petersson, H. Nakatsuji, M. Caricato, X. Li, H. P. Hratchian, A. F. Izmaylov, J. Bloino, G. Zheng, J. L. Sonnenberg, M. Hada, M. Ehara, K. Toyota, R. Fukuda, J. Hasegawa, M. Ishida, T. Nakajima, Y. Honda, O. Kitao, H. Nakai, T. Vreven, J. A. Montgomery, Jr., J. E. Peralta, F. Ogliaro, M. Bearpark, J. J. Heyd, E. Brothers, K. N. Kudin, V. N. Staroverov, R. Kobayashi, J. Normand, K. Raghavachari, A. Rendell, J. C. Burant, S. S. Iyengar, J. Tomasi, M. Cossi, N. Rega, J. M. Millam, M. Klene, J. E. Knox, J. B. Cross, V. Bakken, C. Adamo,

Journal Pre-proofs

J. Jaramillo, R. Gomperts, R. E. Stratmann, O. Yazyev, A. J. Austin, R. Cammi, C. Pomelli, J. W. Ochterski, R. L. Martin, K. Morokuma, V. G. Zakrzewski, G. A. Voth, P. Salvador, J. J. Dannenberg, S. Dapprich, A. D. Daniels, Ö. Farkas, J. B. Foresman, J. V. Ortiz, J. Cioslowski, D. J. Fox, Gaussian 16 Revision A.03, gaussian Inc. Wallingford CT 2016.

[12] M. Kállay, Z. Rolik, J. Csontos, P. Nagy, G. Samu, D. Mester, J. Csóka, B. Szabó, I. Ladjánszki, L. Szegedy, B. Ladóczki, K. Petrov, M. Farkas, P. D. Mezei, H. B, MRCC, a quantum chemical program suite www.mrcc.hu.

[13] R. L. Martin, Natural transition orbitals, J. Chem. Phys. 118 (2003) 4775.

[14] A. A. Shvartsburg, M. F. Jarrold, An exact hard-spheres scattering model for the mobilities of polyatomic ions, Chem. Phys. Lett. 261 (1) (1996) 86--91.

[15] I. Campuzano, M. F. Bush, C. V. Robinson, C. Beaumont, K. Richardson, H. Kim, H. I. Kim, Structural characterization of drug-like compounds by ion mobility mass spectrometry: Comparison of theoretical and experimentally derived nitrogen collision cross sections, Anal. Chem. 84 (2) (2012) 1026--1033.

[16] B. H. Besler, K. M. Merz, Jr., P. A. Kollman, Atomic charges derived from semiempirical methods, J. Comp. Chem. 11 (1990) 431--439.

[17] J. R. Barker, Multiple-well, multiple-path unimolecular reaction systems. I. MultiWell computer program suite, Int. J. Chem. Kinet. 33 (2001) 232--245.

[18] J. R. Barker, Energy transfer in master equation simulations: A new approach, Int. J. Chem. Kinet. 41 (2009) 748--763.

[19] J. R. Barker, T. L. Nguyen, J. F. Stanton, C. Aieta, M. Ceotto, F. Gabas, T. J. D. Kumar, C. G. L. Li, L. L. Lohr, A. Maranzana, N. F. Ortiz, J. M. Preses, J. M. Simmie, J. A. Sonk, P. J. Stimac, J. R. Barker, MultiWell-2017 software suite, University of Michigan, Ann Arbor, Michigan, USA, http://clasp-research.engin.umich.edu/multiwell/ (2017).

[20] J. N. Bull, M. S. Scholz, E. Carrascosa, G. da Silva, E. J. Bieske, Double molecular photoswitch driven by light and collisions, Phys. Rev. Lett. 120 (2018) 223002.

Journal Pre-proofs

[21] J. N. Bull, M. S. Scholz, N. J. A. Coughlan, A. Kawai, E. J. Bieske, Monitoring isomerization of molecules in solution using ion mobility mass spectrometry, Anal. Chem. 88 (2016) 11978--11981.

Journal Pre-proofs